Brain Struct Funct (2015) 220:1477–1496
DOI 10.1007/s00429-014-0739-3

ORIGINAL ARTICLE

The noradrenergic projection from the locus coeruleus to the cochlear root neurons in rats

Sebastián Hormigo · Ricardo Gómez-Nieto · Orlando Castellano · M. Javier Herrero-Turrión · Dolores E. López · José de Anchieta de Castro e Horta-Júnior

Received: 13 December 2013 / Accepted: 17 February 2014 / Published online: 13 March 2014

Abstract The cochlear root neurons (CRNs) are key components of the primary acoustic startle circuit; mediating auditory alert and escape behaviors in rats. They receive a great variety of inputs which serve to elicit and modulate the acoustic startle reflex (ASR). Recently, our group has suggested that CRNs receive inputs from the locus coeruleus (LC), a noradrenergic nucleus which participates in attention and alertness. Here, we map the efferent projection patterns of LC neurons and confirm the existence of the LC-CRN projection using both anterograde and retrograde tract tracers. Our results show that each LC projects to the CRNs of both sides with a clear ipsilateral predominance. The LC axons terminate as small endings distributed preferentially on the cell body and primary dendrites of CRNs. Using light and confocal microscopy, we show a strong immunoreactivity for tyrosine hydroxylase and dopamine β-hydroxylase in these terminals, indicating noradrenaline release. We further studied the noradrenergic system using gene expression analysis (RT-qPCR) and immunohistochemistry to detect specific noradrenergic receptor subunits in the cochlear nerve root. Our results indicate that CRNs contain a noradrenergic receptor profile sufficient to modulate the ASR, and also show important gender-specific differences in their gene expression. 3D reconstruction analysis confirms the presence of sexual dimorphism in the density and distribution of LC neurons. Our study describes a coerulean noradrenergic projection to the CRNs that might contribute to neural processes underlying sensory gating of the ASR, and also provides an explanation for the gender differences observed in the behavioral paradigm.

Keywords Acoustic startle reflex · Gender differences · Neuronal tracers · Noradrenergic receptors · Sensory gating · 3D reconstruction

S. Hormigo and R. Gómez-Nieto contributed equally to this work.

Electronic supplementary material The online version of this article (doi:10.1007/s00429-014-0739-3) contains supplementary material, which is available to authorized users.

S. Hormigo · R. Gómez-Nieto · O. Castellano · M. J. Herrero-Turrión · D. E. López (✉)
Neuroscience Institute of Castilla y León, University of Salamanca, 37007 Salamanca, Spain
e-mail: lopezde@usal.es

S. Hormigo · R. Gómez-Nieto · O. Castellano · D. E. López
Institute of Biomedical Research of Salamanca (IBSAL), University of Salamanca, Salamanca, Spain

R. Gómez-Nieto · O. Castellano · D. E. López
Department of Cell Biology and Pathology, University of Salamanca, Salamanca, Spain

J. de Anchieta de Castro e Horta-Júnior (✉)
Department of Anatomy, Biosciences Institute, São Paulo State University-UNESP, Botucatu, São Paulo 18618-970, Brazil
e-mail: anchieta@ibb.unesp.br

Introduction

The cochlear root neurons (CRNs), found in certain rodents and marsupial species, are located laterally and rostrally in the cochlear nerve root which lies deep within the internal auditory meatus (Harrison et al. 1962; López et al. 1993; Aitkin 1996). Morphologically, they are neurons with a large cell body and thick dendrites which distribute among the eighth nerve fibers (Merchán et al. 1988). CRNs are a specialized neuronal type that mediate alert and escape behaviors driven by sounds, including the acoustic startle and pinna reflexes (López et al. 1999; Horta-Júnior et al.

2008). CRNs convey short-latency acoustic input to giant neurons of the pontine reticular nucleus which, in turn, send information to facial, cranial, and spinal motoneurons (López et al. 1999; Sinex et al. 2001; Nodal and López 2003). This neuronal pathway comprises the primary acoustic startle circuit which makes possible the rapid contraction of skeletal and facial muscles in response to a sudden loud auditory stimulus (Lee et al. 1996; López et al. 1999). The acoustic startle reflex can be modulated by sensory stimuli through sensory gating processes (prepulse inhibition), by non-associative learning processes such as habituation and sensitization, and by emotions such as fear (fear-potentiated startle) and joy (joy-attenuated startle). Prepulse inhibition is the attenuation of the acoustic startle response by a preceding non-startling sensory stimulus, whereas repeated presentation of a robust acoustic startle stimulus exhibits both a decremental process called habituation and an opposing, independent and superimposed incremental process called sensitization (Groves and Thompson 1970; Hoffman and Ison 1980). Since the acoustic startle reflex and its modulations can be easily tested in humans and rats, they provide an animal model with high validity for the study of important human disorders which are characterized by attentional and information-processing dysfunctions (Swerdlow and Geyer 1998; Braff and Geyer 1990; Swerdlow et al. 2001; Fendt et al. 2001; Li et al. 2009; Molina et al. 2009). CRN responses are strongly inhibited by auditory prepulses, and hence, it has been suggested that CRNs are involved in the auditory prepulse inhibition of the acoustic startle reflex (Gómez-Nieto et al. 2010, 2013). Thus, determining the source of inputs to the CRNs is essential to understand the neuronal mechanisms underlying modulation of the acoustic startle reflex in the rat (Gómez-Nieto et al. 2008a, b, 2013). Recently, our group has suggested that the CRNs might receive inputs from the locus coeruleus (LC) (Gómez-Nieto et al. 2008b). The LC is the major noradrenergic nucleus of the brain which participates in behavioral states of high arousal and vigilance, and has a key role in stress responses (Amaral and Sinnamon 1977; Foote et al. 1991; Aston-Jones et al. 1999; Berridge and Waterhouse 2003; Samuels and Szabadi 2008). The knowledge of the outputs of this nucleus has changed gradually as the pathways involving the LC have been defined in great detail. The LC has previously been thought to project diffusely and non-specifically to widespread areas of the brain and spinal cord (Nitecka et al. 1980; Unnerstall et al. 1984). With the advent of more refined techniques, it has become clear that the projections of the LC are extremely selective (Foote et al. 1983; Loughlin et al. 1986a, b; Hormigo et al. 2012). This study aims to investigate whether LC neurons selectively innervate the cochlear root nucleus by determining their distribution projection pattern and neurochemical features, as well as the noradrenergic receptor subtypes in the CRNs. Interestingly, the acoustic startle reflex and its prepulse inhibition are found to be sexually dimorphic in humans and rats (Lehmann et al. 1999; Braff et al. 2001; Aasen et al. 2005). Thus, our study also aims to analyze the gene expression of adrenergic receptors in the female and male cochlear root nucleus to search for neuroanatomical evidence that might explain the gender-specific differences observed in sensory gating of the acoustic startle reflex.

Materials and methods

Experimental animals

In total, 76 adult female and male Wistar rats (Charles River Laboratories) weighing 290–320 g were used in this study. The experiments were conducted in compliance with the guidelines for the use and care of laboratory animals of the European Communities Council Directive (2010/63/EU) and with those established by the Bioethics Committees of the University of Salamanca and São Paulo State University-UNESP. For the surgical procedures, the animals were deeply anesthetized with a mixture of ketamine (40 mg/kg body weight) and xylazine (7 mg/kg body weight). Suffering of the animals was minimized during the surgery by monitoring the depth of anesthesia carefully. Supplementary doses of anesthetic were administrated as required to maintain deep anesthesia throughout the duration of the experiment.

Tract-tracing experiments

A total of 17 animals were used to study the LC-CRN projection. Nine rats received unilateral or bilateral injections of the bidirectional tracer, biotinylated dextran amine (BDA, 10,000 MW; #D-1956; Molecular Probes, Eugene, OR) into the LC. Two of the animals with unilateral BDA injections were analyzed using confocal microscopy to study colocalization of markers, the rest of the cases were examined by light microscopy (see below). In another set of experiments, eight animals were injected with the retrograde tracer, FluoroGold (FG; Fluorochrome, Denver, CO) into the left cochlear root nucleus. All surgical and stereotaxic procedures for injecting the neuronal tracers were identical to those used in our previous studies (López et al. 1999; Gómez-Nieto et al. 2008a, b; Horta-Júnior et al. 2008; Hormigo et al. 2012). Both BDA (10 % in distilled water) and FG (4 % in saline) were injected iontophoretically via a glass micropipette (25 μm tip diameter), with 3 μA positive current pulses (7 s on/7 s off) for a period of 10 min. The coordinates to target the LC were successfully

Table 1 List of antibodies and dilutions used in the immunohistochemistry techniques

Antigen	Primary antibody[a]	Catalog/ brand[b]	Dilution	Secondary antibody	Dilution	Catalog/ brand*	Processing	References
FG	Rabbit anti-FG	#AB-153/ Chemicon	1:2,000	Biotinylated goat anti-rabbit	1:200	#BA-1000/ Vector	LM	Gómez-Nieto et al. (2008a); Horta-Júnior et al. (2008)
TH	Mouse anti-TH	#22941/ Diasorin	1:10,000	Biotinylated goat anti-mouse	1:200	#BA-2000/ Vector	LM	Hormigo et al. (2012)
				Goat Cy5 anti-mouse IgG	1:250	#115-175-003/JI	CM	
DBH	Rabbit anti-DBH	#DZ1020/ BML	1:500	Biotinylated goat anti-rabbit	1:200	#BA-1000/ Vector	LM	Hormigo et al. (2012); Kritzer (2003)
				Goat Cy5 anti-rabbit IgG	1:250	#111-175-003/JI	CM	
				Goat Cy2 anti-rabbit IgG	1:250	#111-225-003/JI	CM	
CaBP	Mouse anti-CaBP	#C-8666/ Sigma	1:200	Biotinylated horse anti-mouse	1:200	#BA-2000/ Vector	LM	Gómez-Nieto et al. (2008a), (b)
				Goat Cy3 anti-mouse	1:250	#115-166-003/JI	CM	
ADR α1	Rabbit anti-ADR α1	PA1-047/ Aff	1:150	Biotinylated goat anti-rabbit	1:200	#BA-1000/ Vector	LM	Vicentic et al. (2002)
ADR α2	Rabbit anti-ADR α2	PA1-048/ Aff	1:150	Biotinylated goat anti-rabbit	1:200	#BA-1000/ Vector	LM	Cai et al. (2013)
ADR β2	Rabbit anti-ADR β2	905-742-100/ADP	1:150	Biotinylated goat anti-rabbit	1:200	#BA-1000/ Vector	LM	Gupta et al. (2007)

[a] Specificity and immunogen sequence of primary antibodies: (1) The anti-FG is a rabbit polyclonal antibody that recognizes the neurotracer FluoroGold (the immunogen was FluoroGold); (2) The anti-TH is a mouse monoclonal antibody that recognizes the 34 kDa catalytic core of TH according to manufacture's studies. The immunogen was full-length TH purified to homogeneity from PC12 cells, which are of rat origin. The antibody has wide species cross-reactivity and was quality control tested using standard immunohistochemical methods; (3) The anti-DBH is a rabbit polyclonal antibody that was produced by using purified DBH from the bovine adrenal medulla as immunogen. This antibody cross-reacts with DBH of human, mouse, rat, cat and bovine origin and has been validated in immunohistochemical or Western blot applications. (4) The anti-CaBP was a mouse IgG isotype produced by hybridization of mouse myeloma cells with spleen cells from mice immunized with calbindin D-28k purified from chicken gut. The antibody specifically stains the 45Ca-binding spot of the calbindin D-28 k (MW 28 kDa) of tissue originating from rat brain in two-dimensional immunoblots; (5) The anti-ADR α1 is a rabbit polyclonal antibody that recognizes the ~60 kDa protein representing the ADR α1a receptor from mouse kidney membrane preparations in immunoblot. The immunogen was a synthetic peptide corresponding to residues K(339) FSREKKAAKT(349) of the 3rd intracellular loop of human ADR α1a; (6) The anti-ADR α2 was an affinity-purified polyclonal rabbit antibody that recognizes the ~45 kDa protein representing ADR α2a receptor from mouse kidney membrane preparations in immunoblot. The immunogen was a synthetic peptide corresponding to residues R(218) I Y Q I A K R R T R V P P S R R G (235) of the 3rd intracellular loop of human ADR α2a; (7) The anti-ADR β2 was an affinity-purified polyclonal rabbit antibody that recognizes human, mouse and rat adrenergic receptor beta2. Predicted MW of ~47 kDa. Higher MW species (~65 kDa) and intermediates also observed by Western blot which reflect post-translational modification of the receptor. The immunogen was a synthetic peptide (SRAPDHDVTQE) of rabbit ADR β2

[b] Antibody manufacturers: ADP, Assay Designs Proteimax (Enzo Life Sciences), São Paulo, Brazil; Aff, Affinity Research Products (Thermo Scientific Pierce Products), Nottingham, UK; BML; Biomol (Enzo Life Sciences), PA, USA; Chemicon, Millipore-Chemicon, Temecula, CA, USA; Diasorin, Stillwater, MN, USA; JI, Jackson Immunoresearch, West Grove, PA, USA; Vector, Vector Laboratories, Burlingame, CA, USA; Sigma, Sigma Aldrich, St. Louis, MO, USA

used in our previous studies (Gómez-Nieto et al. 2008b; Hormigo et al. 2012), and were precisely the same as those devised by Fritschy and Grzanna (1990). The stereotaxic guidance for the left cochlear root nucleus was based on our previous reports (López et al. 1999; Gómez-Nieto et al. 2008a; Horta-Júnior et al. 2008). Following the neurotracer injection, the micropipette was left in place for an additional 15 min prior to withdrawal in order to minimize

leakage of the tracer along the injection tract. After that, the scalp was sutured and the animal was allowed to recover for a minimum of 7 days. Tissue preparation for light microscopy including perfusion of the animals, brain dissection and slicing, visualization of the neurotracers, and calbindin protein-D28K (CaBP) immunohistochemistry was identical to those used elsewhere (López et al. 1993, 1999; Gómez-Nieto et al. 2008a, b). CaBP has been extensively utilized for detecting the cell body, dendrites and axon of the CRNs (López et al. 1993). Thus, a nickel-intensified peroxidase reaction was developed for BDA visualization in order to distinguish it from CaBP-immunohistochemistry, in which heavy-metal intensification of DAB was not applied (Gómez-Nieto et al. 2008a). Cases with injections of FG were initially inspected using a Leica DMRB microscope equipped with epifluorescence to assess the location of the injection site and labeled neurons. In selected cases, FG was converted to a permanent staining by immunohistochemistry on free-floating sections followed by incubation in the avidin–biotin–peroxidase complex (Vectastain, Vector Labs.) and standard histochemistry for peroxidase without heavy-metal intensification (Gómez-Nieto et al. 2008a; Horta-Júnior et al. 2008). Table 1 summarizes the source and working dilutions of antibodies used for light microscopic detection of FG-labeled neurons. All sections were mounted on slides and four alternate series were counterstained with cresyl violet to highlight cytoarchitectonic divisions; the other sections were dehydrated in ethanol and coverslipped with Entellan Neu (#107961; Merck, Darmstadt, Germany).

Immunohistochemistry for catecholamine-synthesizing enzymes and adrenoreceptors

Four animals were used to study the pattern of tyrosine hydroxylase (TH) or dopamine-β-hydroxylase (DBH) immunoreactivity in the cochlear root nucleus. For these experiments, we combined immunolabeling for either TH or DBH with CaBP-immunohistochemistry. After perfusion of the animals and cutting the brain into serial coronal sections of 40 μm thick (Hormigo et al. 2012), we followed a standard immunostaining protocol which included incubation with primary antibody anti-TH or anti-DBH for 72 h at 4 °C. The tissue was then washed and incubated with its corresponding biotinylated secondary antibody for 2 h at room temperature, and finally visualized with the avidin–biotin–peroxidase complex procedure (Vectastain, Vector Labs.) and histochemistry for peroxidase with heavy-metal intensification. After that, CaBP-immunohistochemistry was developed without nickel-intensified peroxidase reaction to yield a brown staining which was clearly distinguishable from the black staining of the TH or DBH immunohistochemistry (Gómez-Nieto et al. 2008a). In another set of experiments, two additional animals were processed according to the procedure described by Gómez-Nieto et al. (2008b) to immunolabel the noradrenergic receptors *α1*, *α2A* and *β2*. Details of the antibodies and their corresponding dilutions are shown in Table 1. In all immunohistochemistry experiments, the omission of the primary antibody resulted in no staining of the preparations. For each brain, all sections were mounted on slides, dehydrated and coverslipped as described above.

Colocalization experiments

In order to determine the codistribution of TH and DBH in the cochlear root nucleus, two animals were used for confocal analysis. In these experiments, we performed double immunofluorescence labeling for the two catecholamine-synthesizing enzymes following a similar procedure to that used in our previous report (Hormigo et al. 2012). After obtaining the brain tissue, free-floating sections (40 μm in thickness) were pretreated with phosphate buffer saline (PBS) 0.3 % Triton X-100 and blocked for 1 h at room temperature with 6 % normal goat serum (#S-1000, Vector Laboratories) in PBS. Subsequently, the brain slices followed overnight incubation at 4 °C with primary antibodies (mouse anti-TH and rabbit anti-DBH, see Table 1 for complete information of antibodies). Thereafter, the sections were rinsed extensively in PBS and incubated for 1 h at room temperature with their corresponding Cy2- or Cy5-conjugated secondary antibodies (Table 1). In another set of experiments, two animals with unilateral injection of BDA were analyzed with confocal microscopy to confirm the colocalization with DBH. In these cases, the BDA was visualized by incubation with Cy2-conjugated streptavidin (dilution 1:650; #016-220-084; Jackson ImmunoResearch), followed by a double immunofluorescence labeling to localize DBH and CaBP as described elsewhere (Gómez-Nieto et al. 2008b). After overnight incubation at 4 °C in a mixture of primary antibodies (rabbit anti-DBH and mouse anti-CaBP), the sections were repeatedly rinsed, and immunoreactivities were visualized with the corresponding combination of affinity-purified secondary antibodies tagged with Cy5 or Cy3 as fluorophores (Table 1). Finally, all sections were rinsed extensively in PBS, dipped briefly in distilled water, mounted onto fluorescence-free slides, air-dried, and coverslipped with Vectashield Mounting Media (#S-1000, Vector Laboratories) to prevent photobleaching. In all colocalization experiments, negative controls were not treated with primary antibodies, and this resulted in the complete absence of immunolabeling.

Isolation of RNA and RT-PCR

The cochlear nerve roots (CNR) of 43 female (24) and male (19) rats were collected bilaterally to study the gene expression of the adrenoreceptor subunits *α1A-C*, *α2A-C* and *β1-3*. Prefrontal cortex (PFC) and hippocampus (H) were also sampled to serve as positive controls. Isolation of RNA and reverse transcription-polymerase chain reaction (RT-PCR) was then performed by standard procedures as described elsewhere (Gómez-Nieto et al. 2008b). Briefly, total RNA was immediately isolated from the individual tissue samples using the TRIZOL® reagent (Gibco BRL, Gaithersburg, MD, USA) in accordance with the manufacturer's procedure. The quantity of purified RNA was assessed by spectrophotometry Nano Photometer (Implen GmbH) and the integrity subsequently confirmed with RNA 6000 Nano LabChip (Agilent Technologies, Palo Alto, CA, USA), obtaining the RNA integrity number (RIN, 0 corresponding to fully degraded RNA and 10 corresponding to intact RNA). For all RT-PCRs, only RNA samples with RIN of at least 7.5 were used, with the vast majority of samples having a RIN of at least 8.0. Subsequently, the total RNA (2 μg), primed with oligo-dT, was reverse-transcribed into complementary DNA (cDNA) at 37 °C for 2 h using the first-strand cDNA synthesis kit (Promega Corporation, Madison, WI, USA) in a 20 μl volume and stored at −20 °C until use, according to manufacturer's instructions. In all cases, a reverse transcriptase negative control was used for testing genomic DNA contamination. PCR reactions were performed in a C1000 Thermal Cycler (Bio-Rad, Spain) and a 25 μl PCR mixture contained 100 ng of cDNA template, 20 pmol of each primer, 0.2 mM dNTPs, 1.5 mM $MgCl_2$ and 5 units of GoTaq Flexi DNA polymerase (Promega Corp.). Supplemental material 1 lists primers specific for the genes examined in the present study. Amplification of rat *β-actin* (GenBank accession No. NM_031144) was used as an internal and loading control. PCRs amplification were as follows: 1 cycle at 95 °C for 5 min as an initial denaturation step, denaturation at 95 °C for 30 s, annealing at 57–60 °C depending on each pair of primers for 30 s, and extension at 72 °C for 45 s (30 cycles), followed by further incubation for 10 min at 72 °C (1 cycle). PCR conditions were shown to be at the linear phase of amplification to assess a semiquantitative analysis. PCR products were electrophoresed on 2.5 % agarose gels in 1 × 40 mM Tris–acetate, 1 mM ethylenediaminetetraacetic acid pH 8.0, and visualized by ethidium bromide staining. The primers were designed in such a way that RT-PCR products spanned two identified introns. Moreover, the amplification of *β-actin* was performed with equal amounts of RNA and demonstrated an identical expression pattern in all cerebral regions used. Finally, in all RT-PCRs, an RNA free (negative) control sample was used which did not produce any amplified bands.

Quantitative real-time PCR (qPCR)

qPCR was performed using the SYBR-Green method with a 2× Master Mix (Applied Biosystems). Each reaction contained 10 μl of Master Mix, 0.4 μl of each pair of primers (see supplemental material 1), 3 μl of each cDNA sample in a different serial cDNA quantity for each gene, and MilliQ water up to 20 μl. The amplification reaction took place in an ABI Prism 7000 detection system (Applied Biosystems), with the following conditions: 10 min at 95 °C followed by 40 cycles of 15 s at 95 °C and 1 min at 60 °C depending on each pair of primers. qPCR experiments were performed in replicates of eight and run in triplicate for each gene product examined. Rat *β-actin* was used as housekeeping gene.

The comparative Ct method was used for presenting quantitative data (Schmittgen and Livak 2008). Following the removal of outliers, raw fluorescence data were used to determine the PCR amplification efficiency (E) according to the formula $E = \left[\left[10^{(-1/\text{slope})}\right] - 1\right] * 100$. All amplifications had an E value of 100 ± 10 % the E value close to 100 % being an indicator of efficient amplification. The relative gene expression value for each transcript was calculated according to the equation $E^{-(\Delta Ct\ \text{“condition 1”} - \Delta Ct\ \text{“condition 2”})}$, where "condition 1" corresponds to males, "condition 2" to samples of females and ΔCt of each "condition" is $Ct_{\text{“experimental gene”}} - Ct_{\text{“endogenous gene”}}$ (Livak and Schmittgen 2001; Schmittgen and Livak 2008). A standard error for each relative gene expression value was calculated as a measure of data variation. Significance from qPCR analysis was determined using a one-way analysis of variance (ANOVA) ($^*p < 0.05$, $^{**}p < 0.01$ or $^{***}p < 0.001$) with a post hoc t Student's test ($^*p < 0.05$, $^{**}p < 0.01$ or $^{***}p < 0.001$).

Three-dimensional reconstructions

Eight animals, 4 males and 4 females, were employed to generate 3-D reconstructions of the LC using Neurolucida (Version 10) and NeuroExplorer (Version 3) software (MicroBrightField Bioscience, Williston, VT, USA). After perfusion of the animal, the brain was collected and a hole was made by the passage of a surgical needle throughout the rostro-caudal plane of the left brainstem. The brains were cryoprotected with sucrose, frozen and serially cut at 40 μm thickness in the coronal plane with a sliding microtome. All sections were mounted on slides, counterstained with cresyl violet, dehydrated and coverslipped as

described above. The outline of cresyl violet-stained coronal sections was viewed with the 5× objective lens of a Leica DMRB microscope and was drawn on the computer screen. Successive sections were aligned via rotation and translation of the drawing with the help of four reference points. The hole, created by the needle, was used for setting one of these reference points, and the other three were set using different anatomical landmarks such as blood vessels, nucleus contours and edges of adjacent sections. All these structures were superimposed and matched in the two successive sections to achieve accurate alignment. After that, the contours of the left and right LC nuclei were manually traced using a 20× objective lens. Finally, LC neurons were identified by their shape and staining intensity and depicted by defining markers of different colors. The contours of the brainstem and LC nuclei were digitized with Neurolucida, and metrically and topologically analyzed with NeuroExplorer. Images and movie documents from the 3D renderings were obtained using Neurolucida software, and 3D models were integrated in PDF documents with Acrobat 9 Pro Extended (Version 9.2.0).

Image and data analysis

The sections processed for light microscopy were examined on an upright brightfield microscope (#BX5; Olympus, Center Valley, PA, USA) equipped with a digital camera (SpotRt®; Diagnostic Instruments, Sterling Heights, MI, USA). Low magnification images were taken with the 4×, 10× or 20× objective lens, and high magnification images were taken with a 40× or 100× objective lens (oil immersion) for morphometric analysis of BDA-labeled structures. The morphometric analysis of labeled structures was carried out with ImageJ (version 1.42; Rasband, N.S., National Institutes of Health, Bethesda, Maryland, USA; http://rsb.info.nih.gov/ij). One case with unilateral injection of BDA into the left LC was selected to illustrate the LC-CRN projection using camera lucida drawings, which were scanned and digitalized with Canvas 7.0 software. For the colocalization experiments, the sections were examined first with a conventional brightfield microscope equipped with fluorescence. In selected slides, the sections were analyzed with a Leica TCS SP2 confocal laser scanning microscope (Leica Microsystems, Mannheim, Germany) coupled to a Leica DM IRE2 inverted microscope and equipped with argon and helium neon lasers with excitation wavelengths of 458, 476, 488, 543, 568, and 633 nm. The fluorochromes Cy2, Cy3, and Cy5 were detected sequentially, stack by stack, with the acousto-optical tunable filter system and triple dichroic mirror TD488/543/633, using laser lines 488, 546, and 633 nm, respectively. The background was controlled, and the photomultiplier voltage (800 V) was selected for maximal sensitivity in the linear range. The objectives used were oil immersion 40× and 63×/numerical aperture 1.30, giving a resolution of 150× nm in the *xy* plane and 300× nm along the *z*-axis (pinhole 1 Airy unit), as well as several electronic zoom factors up to 1.58×. To determine the codistribution of the immunolabeled terminals, series of 25–50 confocal images were obtained to generate a maximal-intensity *z* projection of stacks and an orthogonal projection (=*xy*, *xz*, *yz* planes, for *z* stacks series). Colocalization of the fluorochromes within positive terminals was verified in the orthogonal view and one confocal image of 1 µm thickness in the *z* plane. All photomicrographs shown in the figures were processed with minor modifications in brightness, contrast and to remove the tissue free background using Adobe Photoshop® CS3 Extended (Version 10.0) and assembled in Canvas 7.0 software.

Results

The coerulean projections to the cochlear root nucleus

To determine whether the LC projects to the cochlear root nucleus, we made bilateral injections of BDA into the LC. BDA injections were relatively small (0.6 ± 0.3 mm in diameter), oval in shape, and were confined to the rostrocaudal extent of the LC without spreading to adjacent nuclei (Fig. 1a–c). No necrosis was observed at the points of the BDA injections. In agreement with previous studies, we found anterograde axonal labeling in auditory brain areas that are well known to be targeted by LC neurons such as the cochlear nucleus (Kromer and Moore 1976; Ebert 1996), the superior olivary complex (Mulders and Robertson 2001) and the inferior colliculus (Klepper and Herbert 1991; Hormigo et al. 2012). We further observed numerous BDA-labeled endings in the cochlear root nucleus of both sides (Fig. 1d, e). The cell bodies and dendrites of CRNs were visualized with CaBP-immunohistochemistry in order to examine the distribution of LC-labeled botouns. We found that the LC axons equally distributed throughout dorsal and ventral portions of the cochlear root nucleus (Fig. 1d, e). These LC axons terminate as small endings (mean area of 1.3 ± 0.6 µm^2 and mean perimeter 4.3 ± 0.9 µm, $n = 113$) which contact preferentially the cell body and primary dendrites of CRNs (Fig. 1d1–e2). To study the axonal trajectory of LC neurons that project to the cochlear root nucleus, we made unilateral injections of BDA into the left LC. These BDA injections were similar in size, shape and location to those performed in cases with bilateral injections. Figure 2 illustrates a representative case in which the course of anterogradely labeled axons and collaterals has been drawn

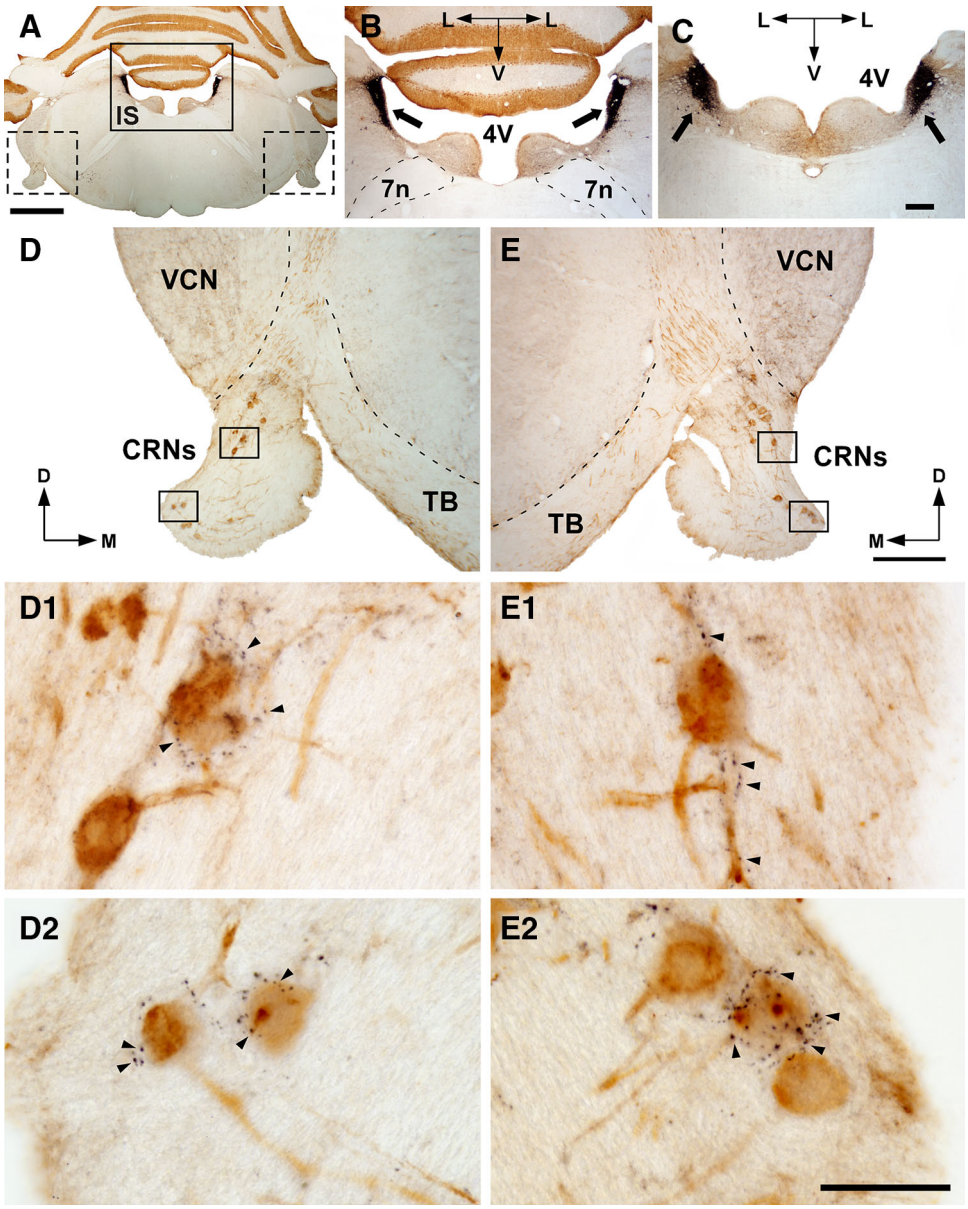

Fig. 1 Bilateral injections of BDA in the locus ceruleus (LC) generate anterogradely labeled endings on the cochlear root neurons (CRNs). **a** Micrograph of a coronal section shows a representative case with bilateral injection sites (IS) in the LC. **b** A higher magnification of the IS (*arrowheads*) corresponding to the frame in (**a**). **c** Micrograph of the rostral part of the BDA injection sites for the same case showed in (**a**). Note the BDA diffusion is confined to the LC. **d** and **e** Micrograph shows the right and left cochlear root nucleus after CaBP immunostaining. The images correspond to the *dashed frames* in (**a**). Higher magnification of the dorsal region (**d1–e1**) and ventral region (**d2–e2**) of the right and left cochlear root nucleus shown in (**d**) and (**e**), respectively. Note numerous LC terminals on cell bodies and primary dendrites (*arrowheads*) of CRNs immunopositive for CaBP. *VCN* ventral cochlear nucleus, *TB* trapezoid body, *4V* fourth ventricle, *7n* facial nerve. *Scale bars* 2 mm in (**a**); 500 µm in (**b**) and (**c**); 500 µm in (**d**) and (**e**); 50 µm in (**d1**, **d2**, **e1**, **e2**)

after BDA injections into the LC. Several heavily labeled bundles were identified close to the injection site (Fig. 2c, d). The LC-labeled axons descend toward the cochlear nucleus following two main pathways. The ipsilateral LC fibers cross the parabrachial nucleus, then, travel caudally between cerebellar peduncle and the vestibular nucleus to continue through the spinal trigeminal nucleus. Some fibers curve laterally and enter the acoustic stria to reach the caudal part of the ventral cochlear nucleus and the cochlear root nucleus (Fig. 2). The contralateral LC fibers descend through the pontine central gray along the rostral tip of the fourth ventricle. These fibers cross the midline, pass the contralateral LC and enter the acoustic stria to reach the ventral cochlear nucleus and the cochlear root nucleus (Fig. 2). We further verified the existence of the LC-CRN projection and assessed its bilateral symmetry by injecting the retrograde tracer FluoroGold (FG) into the left cochlear root nucleus (Fig. 3; Supplemental material 2). The injection sites were large (0.8 ± 0.4 mm in diameter) and restricted to the cochlear nerve root (Fig. 3a). As expected, we found retrogradely labeled neurons in the LC of both sides (Fig. 3b; Supplemental material 2). The number of FG-labeled neurons located on the ipsilateral LC (76 ± 18 %) was considerably higher than on the contralateral LC (24 ± 18 %), and were distributed preferentially in the caudal part of the LC (e. g. in Fig. 3c, d). These results demonstrate that the LC projects to the CRNs with a clear ipsilateral preference.

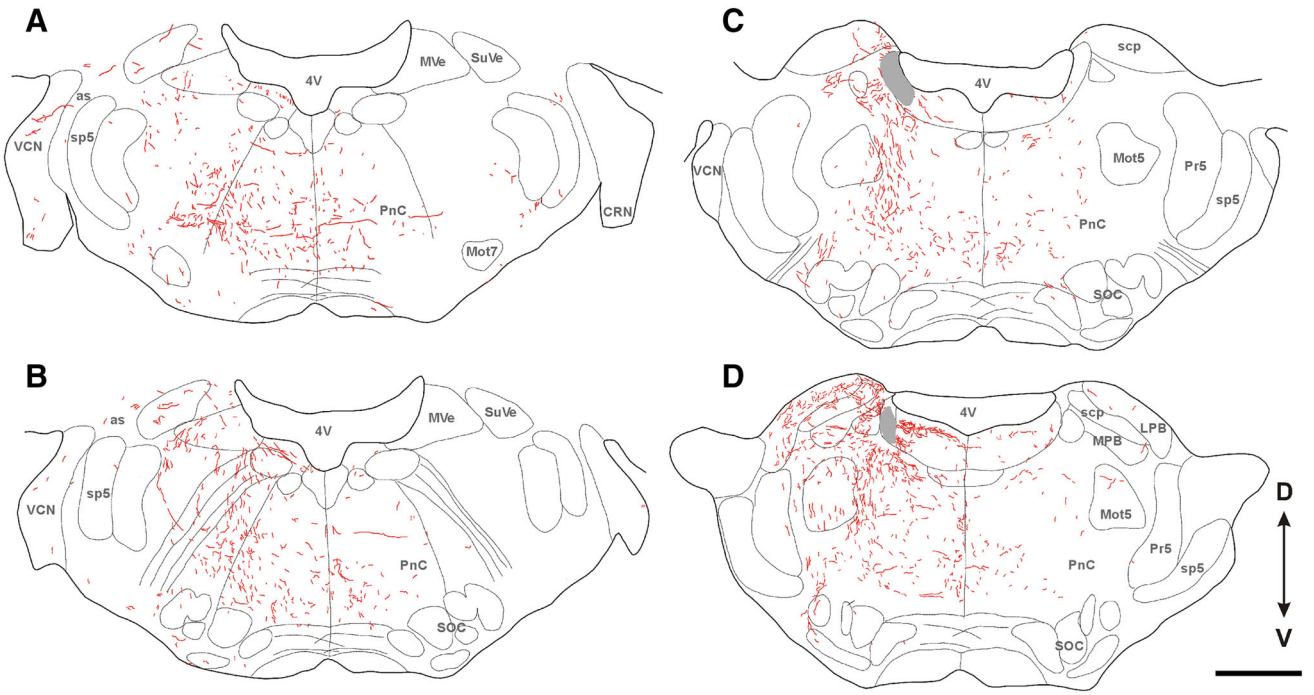

Fig. 2 The coerulean pathway to the cochlear root neurons. Camera lucida drawings of coronal sections show distribution of anterogradely labeled axons and collaterals (BDA, *red*) after BDA injections into the LC (*gray*). Drawings are arranged from caudal to rostral (**a–d**) and are regularly spaced at 400 µm intervals. *as* acoustic stria, *CRN* cochlear root nucleus, *LPB* lateral parabrachial nucleus, *Mot5* motor trigeminal nucleus, *Mot7* trigeminal motor nucleus, *MPV* medial parabrachial nucleus, *MVe* medial vestibular nucleus, *PnC* caudal pontine reticular nucleus, *Pr5* principal sensory trigeminal nucleus, *SOC* superior olivary complex, *scp* superior cerebellar peduncle, *sp5* spinal trigeminal nucleus, *SuVe* superior vestibular nucleus, *VCN* ventral cochlear nucleus, *4V* fourth ventricle. *Scale bar* 1 mm

TH and DBH immunoreactivity in the cochlear root nucleus

To assess the catecholaminergic content of the cochlear root nucleus, we combined immunolabeling for tyrosine hydroxylase (TH) or dopamine-β-hydroxylase (DBH) with CABP-immunohistochemistry (Figs. 4, 5). In cases with TH immunochemistry, a heavy immunoreactive staining of neurons and fibers was seen in the LC (Fig. 4a). We further observed many darkly staining varicosities along the labeled fibers as they coursed from dorsal to ventral areas of the cochlear root nucleus (Fig. 4b). These terminals were found in close apposition to the cell body and dendrites of CRNs which were displayed with CaBP-immunohistochemistry (Fig. 4c, d; Supplemental material 3A-B). Putative noradrenergic fibers and terminals were further identified by means of immunohistochemical detection of DBH, the final enzyme in the biosynthetic pathway of noradrenaline. The LC showed dense staining of DBH immunoreactivity which was similar but not identical to TH immunoreactivity (Fig. 5a). As it was noted in cases with TH immunoreactivity, DBH-immunoreactive fibers and varicosities were also equally dense throughout the dorsoventral length of the cochlear root nucleus (Fig. 4b). The DBH-immunolabeled terminals distributed onto the cell body and dendrites of CRNs immunolabeled for CaBP (Fig. 5c, d; Supplemental material 3C-D). Additionally, we studied the codistribution of TH and DBH-immunoreactive terminals in the cochlear root nucleus by double immunofluorescent staining and colocalization analysis (Fig. 6; Supplemental material 4). TH and DBH-immunoreactive terminals were found in the cochlear root nucleus with a distribution similar to that with single immunolabeling (Fig. 6; Supplemental material 4). The orthogonal view (Fig. 6d) and 1-µm confocal images (Supplemental material 4D) confirmed that TH and DBH terminals colocalized.

The LC projection to CRNs is noradrenergic

To determine whether the LC projection to the CRNs uses noradrenaline as neurotransmitter, we measured the terminals immunolabeled for TH or DBH, and compared their size and distribution pattern to those labeled with BDA after injection in the LC. Comparing the results of both experiments, we observed that the number of TH and

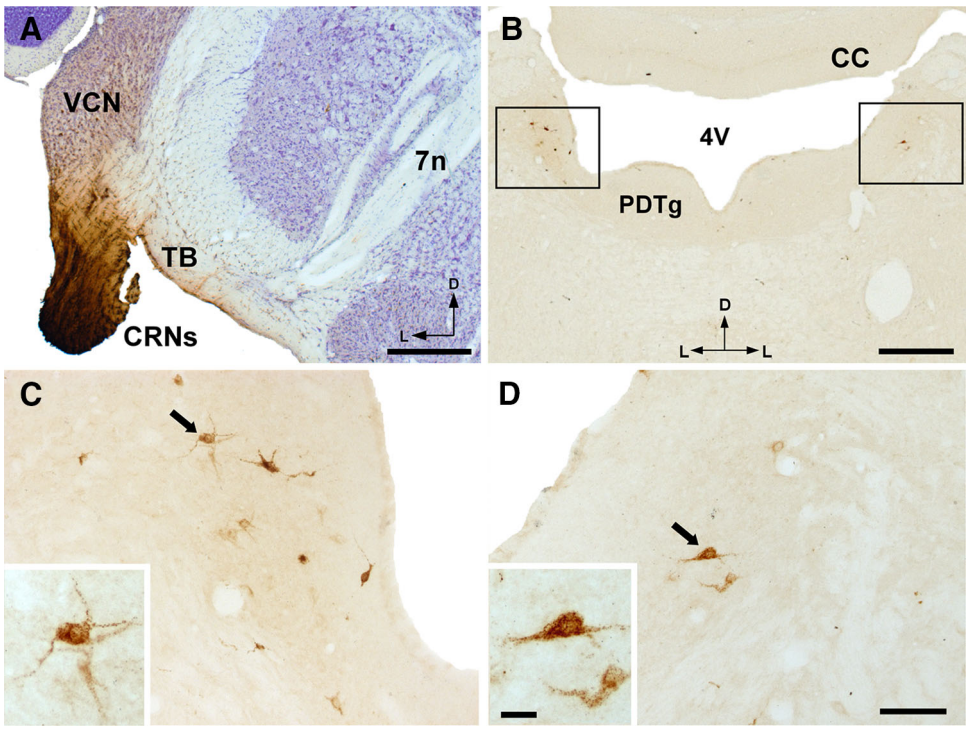

Fig. 3 Locus ceruleus (LC) neurons are retrogradely labeled following injections of FluoroGold (FG) into the cochlear root nucleus. **a** Micrograph of a Nissl-counterstained coronal section shows the center of the injection sites. **b** Retrogradely labeled neurons in the LC of both sides. Notice that there are more retrogradely labeled neurons in the ipsilateral than in the contralateral side. **c** and **d** High magnification micrographs (corresponding to the frame in **b**) shows FG-labeled LC neurons in the ipsilateral (**c**) and contralateral LC. FG-labeled LC neurons are large with fusiform or polygonal cell bodies, and display filling of their dendritic trees (see insets corresponding to the *arrow* in **c** and **d**). *CC* cerebellar cortex, *CRNs* cochlear root neurons, *PDTg* posterodorsal tegmental nucleus, *VCN* ventral cochlear nucleus, *TB* trapezoid body, *7n* facial nerve, *4V* fourth ventricle. *Scale bars* 500 μm in (**a**) and (**b**); 100 μm in (**c**) and (**d**) (25 μm in the insets)

DBH-immunolabeled terminals was considerably higher than those labeled with BDA (for comparison see Figs. 1, 4, 5). TH and DBH-immunolabeled terminals had a mean area of 1.4 ± 0.5 μm^2 and mean perimeter of 4.5 ± 0.8 μm ($n = 137$); therefore, their size were very similar to the LC terminals labeled with BDA. The distribution pattern of TH and DBH-immunolabeled terminals throughout the cochlear root nucleus also resembled that described for the LC-BDA terminals. In both experiments, we observed that the labeled fibers terminate in numerous endings onto the cell bodies and primary dendrites of CRNs (for comparison see Figs. 1, 4, 5). We verified that the LC projection to the CRNs is noradrenergic by using a triple-labeling method consisting of BDA injection into the LC combined with double immunofluorescence for DBH and CaBP (Fig. 7). In these experiments, we observed colocalization of the tracer with DBH-immunoreactive endings which terminate on CRNs immunolabeled for CaBP (Fig. 7d). These results suggest that the coerulean projection to the cochlear root nucleus is noradrenergic.

Gene expression of noradrenergic receptors in the cochlear root nucleus

Our immunohistological study suggested that CRNs are under the influence of noradrenaline. These results led us to investigate the noradrenergic receptor machinery of CRNs, and hence, we focused on determining the gene expression of adrenoreceptors in the cochlear nerve root. We performed RT-PCR analysis for nine selected genes (Supplemental material 1) and found that the cochlear nerve root expressed the adrenoreceptor subunits *α2A-C* and *β1-3* (Fig. 8a), a result which was consistent with our previous study (Gómez-Nieto et al. 2008b). We further detected the adrenoreceptor subunits *α1A-C* (Fig. 8a). The majority of these genes also showed a marked expression level in cells of the prefrontal cortex (PFC) and/or hippocampus (H), and hence, we used them as positive control. The gene expression level of the noradrenergic receptors *α1B*, *α2A*, *α2B*, *β2*, and *β3* was relatively high, whereas the adrenoreceptor subunits *α1A*, *α1C*, *α2C*, and *β1* showed the lowest expression levels. Additionally, we verified the presence of

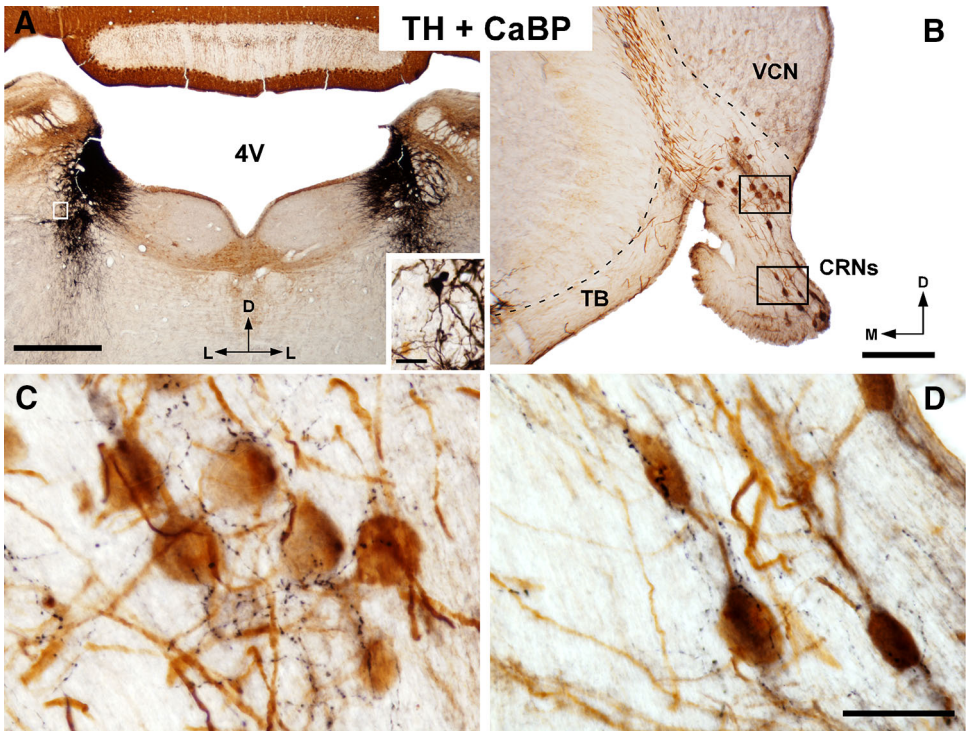

Fig. 4 Tyrosine hydroxylase (TH) immunoreactivity in the cochlear root nucleus. **a** Micrograph of a coronal section through the center of the LC shows TH and CaBP immunolabeling. The TH immunoreactivity appears as an intense black reaction product. The inset shows a higher magnification of an LC neuron (corresponding to the *white frame*). **b** Low magnification micrograph shows the cochlear root nucleus after TH and CaBP immunolabeling. **c**, **d**, Higher magnification of the dorsal (**c**) and ventral (**d**) regions of cochlear root nucleus (corresponding to the frames in **b**) shows TH-immunolabeled endings (in *black*) on the cochlear root neurons (CRNs) immunolabeled for CaBP (in *brown*). Note small and numerous beaded endings terminated preferentially on the cell body and primary dendrites of CRNs. *TB* trapezoid body, *VCN* ventral cochlear nucleus, *4V* fourth ventricle. *Scale bars* 1 mm in (**a**) (25 μm in the inset); 500 μm in (**b**); 50 μm in (**c**) and (**d**)

α1, *α2A* and *β2* adrenoreceptor proteins in the CRNs by means of immunohistochemistry staining (Fig. 8b). Strong-to-moderate staining of those adrenoreceptors was observed with cytoplasmatic and membranous distribution in the cell bodies and primary dendrites of CRNs (Fig. 8b). The immunohistochemical staining correlated with the results obtained with the RT-PCR method and suggested that the CRNs contain a noradrenergic receptor profile sufficient to respond to LC inputs.

Gender differences in gene expression of adrenoreceptors in the cochlear nerve root

An important characteristic of the acoustic startle reflex and its modulations is that they show a marked sexual dimorphism. As mentioned above, our RT-PCR analysis suggested that the CRN projection might contain adrenoreceptors that modulate the acoustic startle reflex. If that is the case, we might encounter gender differences in the adrenoreceptor profiles expressed in the cochlear nerve root. To determine whether there are the sex differences in the expression levels of adrenoreceptors in the cochlear nerve root, we performed a quantitative reverse transcription real-time PCR (RT-qPCR) analysis in female and male rats (Fig. 9). We observed a marked gender difference in the expression levels of adrenoreceptors, except for the gene encoding the subunit *α1B* which showed a tendency for increased expression in females without a significant difference (Fig. 9a). According to the RT-qPCR analysis, the subunits *α1A*, *α2C*, *β1* and *β1* were expressed predominantly in male rats. Especially noteworthy is the gene expression level of the subunit *β1* which was 47 times greater than that seen in females (Fig. 9c). Significant differences in the subunits *α1A* and *α2C* were also found ($p < 0.001$), showing overexpression in males as compared to females (Fig. 9a, b). In contrast, gene expression levels of the subunits *α1C*, *α2A*, *α2B* and *β3* were significantly higher in females than males. The subunits *α1C*, *α2A* and *β3* showed the highest mRNA expression levels in females as compared to males ($p < 0.001$). In sum, the noradrenergic receptors showed a sex-linked differential gene expression in the cochlear nerve root.

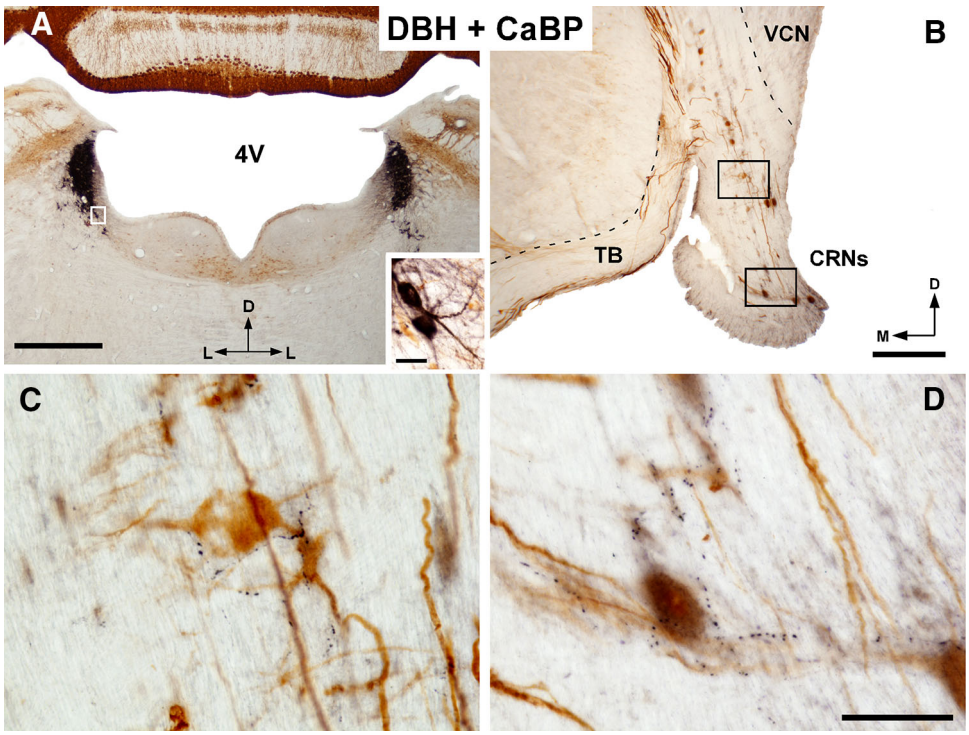

Fig. 5 Dopamine β-hydroxylase (DBH) immunoreactivity in the cochlear root nucleus. **a** Micrograph of a coronal section through the center of the LC shows DBH and CaBP immunolabeling. The DBH immunoreactivity appears as an intense black reaction product. The inset shows a higher magnification of an LC neuron (corresponding to the *white frame*). **b** Low magnification micrograph shows the cochlear root nucleus after DBH and CaBP immunolabeling. **c**, **d** Higher magnification of the dorsal (**c**) and ventral (**d**) regions of cochlear root nucleus (corresponding to the frames in **b**) shows DBH-immunolabeled endings (in *black*) on the cochlear root neurons (CRNs) immunolabeled for CaBP (in *brown*). Note small and numerous beaded endings terminated preferentially on the cell body and primary dendrites of CRNs. *TB* trapezoid body, *VCN* ventral cochlear nucleus, *4V* fourth ventricle. *Scale bars* 1 mm in (**a**) (25 µm in the inset); 500 µm in (**b**); 50 µm in (**c**) and (**d**)

Gender differences in the distribution of LC neurons

The RT-qPCR analysis showed that CRNs might display sexual dimorphism in noradrenergic receptor expression and our tract-tracing experiments indicated that the noradrenergic neurons projecting to CRNs are distributed preferentially in the caudal part of the LC. In an attempt to determine morphological sex differences that might be linked to the LC-CRN projection, we performed a 3D reconstruction analysis of the LC in female and male animals (Fig. 10). The total volume of the LC showed no difference between females and males (Fig. 10a, b). We observed that females had more LC neurons than males; however, we found no significant differences in the total density of LC neurons between females and males (Fig. 10c). The LC of female animals showed a neuronal density of 39,559 ± 2,014 neurons per mm^3, whereas males showed an average numerical density of 38,140 ± 2,734 neurons per mm^3. Despite the resemblance in the total volume and neuronal density, we observed that neuronal density clearly differs throughout the rostro-caudal length of the LC in each sex (Fig. 10d). The number of LC neurons was significantly higher in the rostral area of the female brain as compared to males ($p < 0.001$), while the LC of males contains higher neuronal density in caudal areas (Fig. 10d). The gender-specific differences in the distribution of LC neuronal density is shown in a contour 3D model with free rotation and zoom (see 3D PDF files in supplemental material 5 and 6 which depicts female and male brainstems, respectively). For better visualization see also movie 1 within the supplementary material.

Discussion

The present study confirms the existence of a direct projection from the LC to the cochlear root nucleus as suggested in our previous report (Gómez-Nieto et al. 2008b). We further provide detailed information about the neuronal pathway and neurochemistry of the LC-CRN projection. The LC neurons send projections to the CRNs of both sides with a marked ipsilateral predominance. These coerulean fibers use noradrenaline as neurotransmitter and give off numerous small endings that contact preferentially the cell

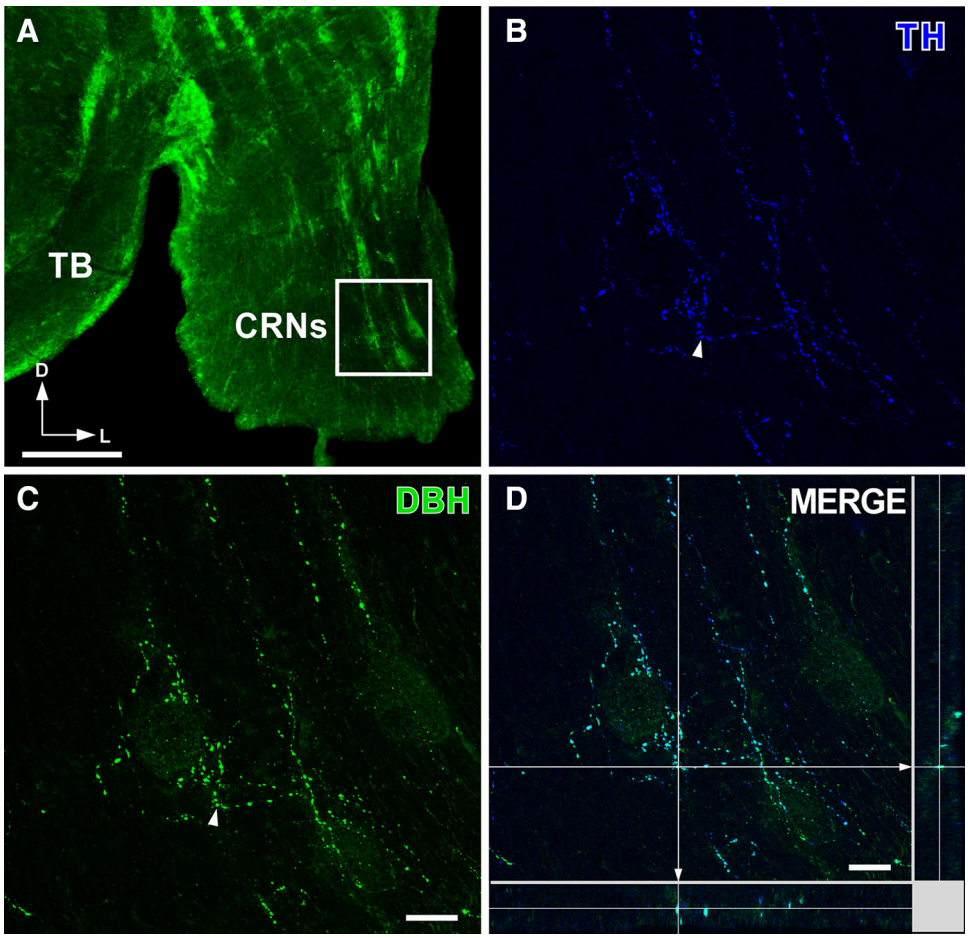

Fig. 6 Colocalization of tyrosine hydroxylase (TH) and dopamine β-hydroxylase (DBH) in the cochlear root nucleus. **a** Fluorescence micrograph shows a coronal section through the center of the cochlear nerve root after DBH immunolabeling. **b** Confocal image of the *boxed area* in (**a**) shows TH-immunolabeled endings (in *blue*, Cy5) in the cochlear root nucleus. **c** Confocal image shows DBH-immunolabeled endings (in *green*, Cy2) in the cochlear root nucleus. **d** Confocal image shows the merge of the maximum *z*-series projection shown in (**b**–**c**). Colocalization of a TH and DBH ending (corresponding to the *arrowhead* in **b**–**c**) is confirmed by the orthogonal view. *CRNs* cochlear root neurons, *TB* trapezoid body. *Scale bars* 200 µm in (**a**); 20 µm in (**b**, **c**, and **d**)

body of CRNs. The CRNs in turn contain the noradrenergic receptor profile sufficient to respond to the LC neurons. Thus, our study supports the idea that the cochlear root nucleus is the first brainstem nucleus that participates not only in the initiation of the acoustic startle reflex (López et al. 1999) but also in its modulation (Gómez-Nieto et al. 2008a, b, 2013). Furthermore, we reported that CRNs exhibit important gender-specific differences in gene expression of adrenoreceptors. This result together with the differences found in the distribution of the LC neuronal density between males and females might help to explain the gender differences observed in the behavioral paradigm (Lehmann et al. 1999).

CRNs receive inputs from the LC

The efferent projections of the LC have been widely studied in the rat by tract-tracing techniques. Thus, it has been previously reported that the LC projects to auditory brain areas such as the cochlear nucleus (Kromer and Moore 1976; Ebert 1996), the superior olivary complex (Mulders and Robertson 2001) and the inferior colliculus (Klepper and Herbert 1991; Hormigo et al. 2012). In our tracing experiments with bilateral injections of BDA in the LC, we have observed all those projections and we further showed that LC neurons send projections onto the CRNs. This result corroborates our earlier observation, which showed that single BDA injections in the LC generate anterograde labeling in the cochlear root nucleus (Gómez-Nieto et al. 2008b). We also verified the existence of the LC-CRN projection by injecting FluoroGold, a pure retrograde tracer, into the cochlear root nucleus. Our FluoroGold injections worked adequately as other known inputs to the CRNs were consistently labeled (Gómez-Nieto et al. 2008a). An important conclusion that we draw from our retrograde tracing experiments is that the LC-CRN projection is mainly ipsilateral. This result is consistent with other studies which found that the inferior colliculus (Hormigo et al. 2012) and the somatosensory thalamic nucleus (Simpson et al. 1997) receive a larger fraction of their LC input from the ipsilateral nucleus. Our report also describes in detail the pathway that projects from the LC to the cochlear root nucleus using BDA tracing. We found similarities between the course of LC

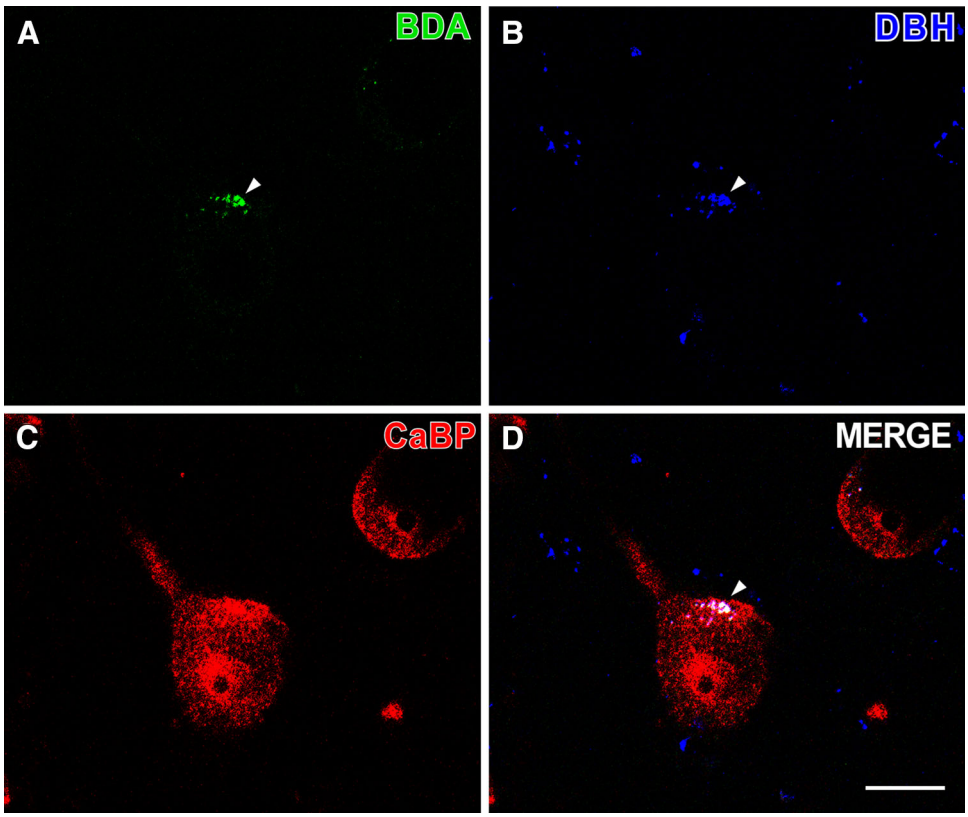

Fig. 7 Noradrenergic terminals from the locus coeruleus (LC) onto the cochlear root neurons (CRNs). **a** Confocal image shows a BDA-labeled ending (in *green*, Cy2, *arrowhead*) in the cochlear root nucleus after injection in the LC. **b** Confocal image of the same area in (**a**) shows DBH-immunolabeled endings (in *blue*, Cy5, *arrowhead*). **c** Confocal image shows a CRN immunolabeled for CaBP (in *red*, Cy3). **d** Merge image of (**a**), (**b**), and (**c**) shows colocalization of BDA and DBH on the same terminal (*arrowhead*) that is in close apposition to the cell body of a CRN. *Scale bars* 20 µm

axons that reach the cochlear root nucleus and the coerulean pathway, described by Kromer and Moore (1980) with autoradiographic tracing, which targets ventral areas of the cochlear nucleus. Although Kromer and Moore (1980) reported an absence of LC fibers in the cochlear nerve, our study clearly demonstrates that the LC also innervates the cochlear root nucleus. This rather contradictory result may be due to the different tracing methods used in each study and the densely myelinated nature of the cochlear nerve which might mask the indirect labeling used in the autoradiographic technique. The CRNs receive a great variety of excitatory and inhibitory inputs (Harrison et al. 1962; Merchán et al. 1988; Osen et al. 1991; Gómez-Nieto et al. 2008a, b). We found that the LC endings were less numerous and considerably smaller than the cholinergic endings from the ventral nucleus of the trapezoid body (Gómez-Nieto et al. 2008a, 2013). The distribution of LC endings was also different; the LC endings distributed preferentially on cell bodies and primary dendrites of CRNs, whereas the cholinergic endings uniformly distributed along the whole neuron including distal dendrites (Gómez-Nieto et al. 2008a). Such differences indicate that LC inputs to CRNs are distinct from other CRN afferents and suggest that CRNs act to integrate information from different sources including non-auditory brain areas.

The noradrenergic system in the cochlear root nucleus

The LC is the principal site for brain synthesis of noradrenaline (Amaral and Sinnamon 1977) and our tracing studies indicates that the CRNs receive LC inputs. Thus, it was interesting to examine the distribution of the catecholamine-synthesizing enzymes (TH and DBH) in the cochlear root nucleus. Our results showed numerous TH- and DBH-immunoreactive fibers and varicosities that were found in close apposition to cell bodies and primary dendrites of CRNs. This accords with our earlier observations (Gómez-Nieto et al. 2008b), which showed TH immunopositive endings in the cochlear root nucleus. Our current study further described in detail the distribution of DBH immunopositive endings on the CRNs. DBH immunoreactivity has been previously found in the rat cochlear nucleus (Klepper and Herbert 1991). These authors reported that fibers immunolabeled for DBH were rare within the cochlear nerve (8n); however, our study demonstrated that DBH fibers profusely innervate the cochlear root nucleus. The fact that the cochlear nerve was not analyzed in all its length in Klepper and Herbert (1991) study might explain why our result was unnoticed. Our study also indicated that the majority of TH-immunoreactive terminals colocalized with DBH. Since the DBH is the final enzyme in the synthetic chain for noradrenaline, converting

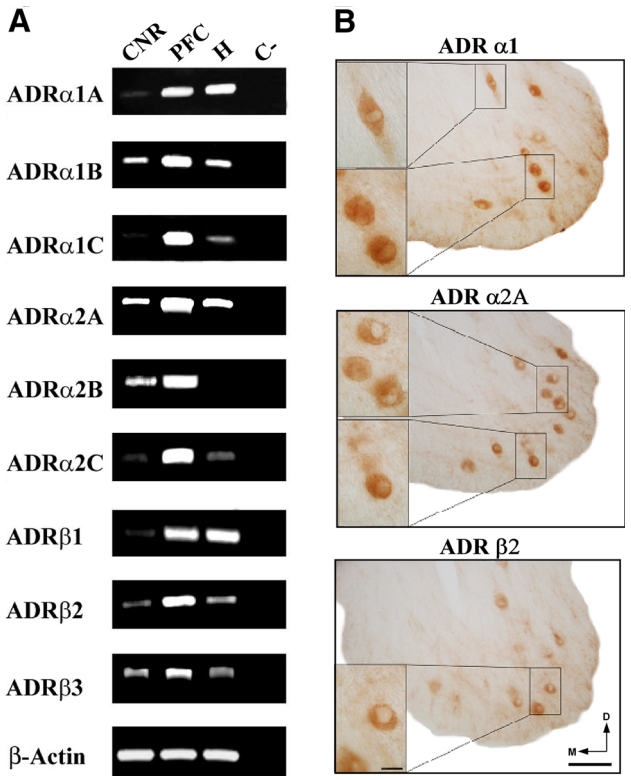

Fig. 8 Noradrenergic receptor types in the cochlear root nucleus. **a** Gene expression levels of noradrenergic receptor types (ADR α1A-C, ADR α2A-C, ADR β1-3) in the cochlear nerve root (CNR), prefrontal cortex (PFC), hippocampus (H) and negative control (C−) in the exponential phase of different PCRs (40 cycles). Primer sequences, sizes of the distinct fragments and conditions of PCRs are detailed in supplemental material 1. β-*actin* was used as control for equal amounts in RT-PCR reactions. **b** Micrographs of noradrenergic receptor immunolabeling (ADR α1, ADR α2A and ADR β2) in the cochlear root nucleus. Insets correspond to higher magnifications of cochlear root neurons. *Scale bars* 100 μm in (**b**) (20 μm in the inset)

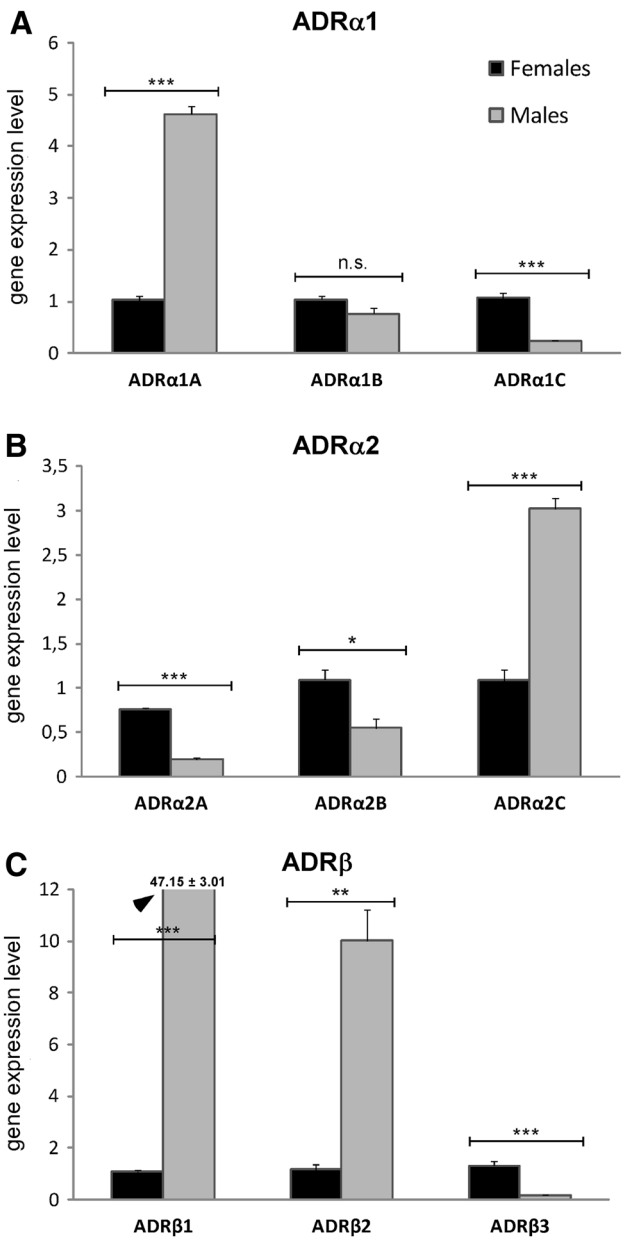

Fig. 9 Gender differences in gene expression of noradrenergic receptors in the cochlear root nucleus. Graphs show gene expression levels of adrenoreceptors (ADR) *α1A-C* (**a**), ADR *α2A-C* (**b**), and ADR *β1-3* (**c**) in female vs. male rats. The mRNA levels were determined by quantitative real-time PCR (qPCR). Notice genes with significantly expression levels between gender groups. Data are mean ± SE and were normalized to female transcripts levels. *n.s.* no significant difference; $*p < 0.05$; $**p < 0.01$; and $***p < 0.001$. Female group with $n = 19$ and male group with $n = 19$

dopamine to noradrenaline, our colocalization study suggests strong noradrenaline release on the CRNs. Several lines of evidence indicate that the noradrenergic input to the CRNs originates from the LC. First, the size of TH or DHB immunolabeled terminals on the CRNs is similar to that of LC-BDA-labeled terminals on these neurons. Second, an equal pattern of terminal distribution throughout the cochlear root nucleus was found for TH or DHB immunolabeled terminals and those from the LC. In fact, all these terminals distributed similarly onto the CRNs, targeting preferentially cell bodies and primary dendrites. Finally, the coerulean origin of noradrenergic inputs to CRNs was confirmed by our triple-labeling experiment consisting of BDA injections in the LC combined with BDH and CaBP immunolabeling. The colocalization analysis indicated that LC-BDA terminals on the CRNs contain the catecholaminergic enzyme DBH. This result is in agreement with Gómez-Nieto et al. (2008b) findings which showed, using a similar approach, colocalization of TH-immunolabeled terminals with LC terminals on CRNs. Accounting for the above results, we conclude that noradrenaline is the neurotransmitter used by the LC-CRN projection. It is interesting to note that the number of LC-BDA terminals on the CRNs was considerably less than the

number of DBH-immunolabeled terminals. This difference was contrary to our expectations as BDA injections into the LC were made bilaterally and a large extent of the nucleus was filled by the tracer. This might suggest that the LC is not the sole source of noradrenergic inputs to the CRNs. In fact, the cochlear nucleus receives projections from the A5 noradrenergic cell group, as well as sparse projections from the A4 and A7 cell groups (Klepper and Herbert 1991). Further research is required to investigate whether these non-coerulean noradrenergic nuclei also send projections to the cochlear root nucleus. To complete the study of the noradrenergic system in the cochlear root nucleus, we analyzed the gene expression of adrenoreceptors in the cochlear nerve. In agreement with earlier findings (Gómez-Nieto et al. 2008b), our data showed that CRNs expressed two main groups of adrenergic receptors, α and β, and specifically the subtypes $\alpha 1A$-B-C, $\alpha 2A$-B-C and β-1-2-3. These results were subsequently confirmed by immunolabeling, suggesting that CRNs contain the adrenoreceptors that are specific targets of the noradrenaline transmitter. Since LC neurons mediate dual effects: neuronal excitation by $\alpha 1$-adrenoceptors and inhibition by $\alpha 2$-adrenoceptors (Szabadi 2013) and CRNs are known to take part in the acoustic startle reflex (Lee et al. 1996; López et al. 1999), the LC-CRN projection might contribute to the modulation of the acoustic startle reflex.

The LC-CRN projection in relation to the acoustic reflex pathways

The CRNs comprise the first nucleus of the primary acoustic startle circuit and are critical in the initiation and full expression of the acoustic startle and pinna reflex (Lee et al. 1996; López et al. 1999; Horta-Júnior et al. 2008). Prior studies have also noted the importance of the cochlear root nucleus in the modulation of the acoustic startle reflex (Gómez-Nieto et al. 2008a, b, 2010, 2013). These studies focused on analyzing the CRN afferents and provided molecular and electrophysiological evidence of their role in the modulation and inhibition of the CRN response after auditory prepulse stimulation. Our current study increases the knowledge of the CRN inputs, suggesting that the coerulean noradrenergic system in the cochlear root nucleus might account for the neuronal mechanism underlying the modulation of the acoustic startle reflex. In fact, several pharmacological experiments indicate that noradrenaline modulates motor outflow in the acoustic startle reflex (Saitoh et al. 1986; Davis et al. 1977; Bakshi and Geyer 1997). As an instance clonidine, an $\alpha 2$-adrenoceptor agonist that significantly reduces activity of LC neurons, has been found to attenuate the amplitude of the acoustic startle reflex, while on the contrary the $\alpha 2$-adrenoceptor antagonist yohimbine, known to increase LC activity, enhances the amplitude of the startle response (reviewed in Samuels and Szabadi 2008; Szabadi 2012). Our real-time PCR experiments demonstrated that CRNs contain the adrenergic receptor subtypes, including the $\alpha 2$-adrenoreceptor, by which those drugs might reduce or increase the amplitude of the acoustic startle reflex. The reduction of the startle response after bilateral chemical lesions of the LC also supports its role in the modulation of behavioral reactivity to sensory stimulation (Adams and Geyer 1981). Our study showed that CRNs receive direct LC inputs, indicating that there are at least two efferent pathways through which LC could modulate the acoustic startle reflex (Fig. 11). The LC noradrenergic axons contact the primary acoustic startle reflex at the initial and final relays of the primary acoustic startle circuit. On the first relay, CRNs contain noradrenergic receptors ($\alpha 1$, $\alpha 2$, $\beta 2$-adrenoreceptors) that are sufficient to modulate the acoustic startle response. On the final relay, motoneurons in the spinal cord are under the influence of excitatory projections from the LC via $\alpha 1$-adrenoreceptors (Szabadi 2012). It is also reasonable to propose that the LC participates, via the coerulean projection to the CRNs, in motor reflexes that accompany the acoustic startle reflex such as the auricular reflex. The LC, which regulates attention, participates in the maintenance of behavioral states of high arousal and vigilance (Aston-Jones and Cohen 2005), and the CRNs are crucial in the auricular reflex which provides stimulus orientation as well as selective attention toward the stimulus source (Landis and Hunt 1939; Horta-Júnior et al. 2008). Thus, CRNs send ipsilateral projections to motoneurons of the facial motor nucleus which in turn innervates the muscles responsible for pinna movement (Horta-Júnior et al. 2008). Since the facial motor nucleus also receives dense innervations from the LC (Jones and Yang 1985), the primary auricular reflex circuit might be also regulated in its initial and final relays by the LC (Fig. 11). Supporting this suggestion, we also found that our BDA injections in the LC generated anterograde labeling in the medial subnucleus of the facial motor nucleus which specifically contains motoneurons that receive CRN inputs (data not shown). Although further research should be done to investigate the functional implications of the LC-CRN projection, it is possible to hypothesize that the LC-CRN projection might participate not only in the modulations of the acoustic startle reflex but also in the neuronal circuits that mediate their regulation as it might occur in the prepulse inhibition. Alsene and Bakshi (2011) have demonstrated, using pharmacological stimulation and inhibition of LC, that the prepulse inhibition paradigm is regulated by the LC noradrenergic system. The activation of LC neuronal firing elevates noradrenaline release in LC terminal regions resulting in a disruption of the prepulse inhibition (Berridge and Abercrombie 1999;

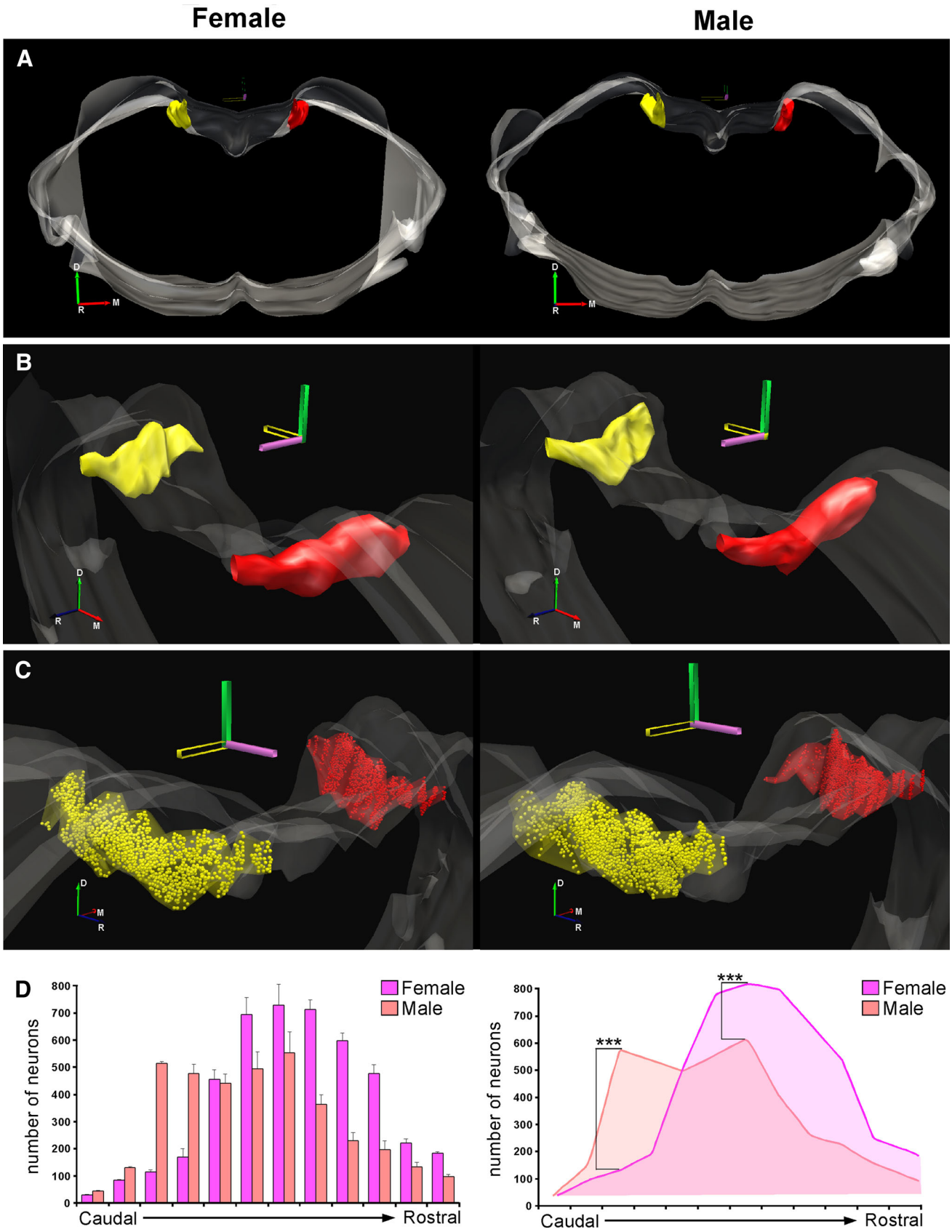
Female
Male
A
B
C
D
D
R
M
number of neurons
800
700
600
500
400
300
200
100
0
Female
Male
Caudal
Rostral
***
***

◀**Fig. 10** Sexual dimorphism in the distribution of coerulean neurons. **a** 3D reconstruction of the female and male brainstem containing the locus coeruleus (LC), seen from a rostral point. The right and left LC have been represented in *yellow* and *red*, respectively. **b** Zoom-in images from the 3D reconstruction in (**a**) shows details of the LC. **c** 3D reconstruction images show distribution of LC neurons along the rostro-caudal plane. Nissl-stained neurons have been represented as *dots*. Note differences in neuronal distribution between female and male. **d** Histograms of the neuronal distribution along the rostro-caudal plane of the female and male LC. Notice significant differences in the number of neurons distributed rostrocaudally between sexes. $***p < 0.001$. Female group with $n = 4$ and male group with $n = 4$

Alsene and Bakshi 2011). Our study provides strong evidence of LC noradrenaline release in the cochlear root nucleus, and therefore, the LC-CRN projection might be part of the noradrenergic pathways that are altered after experimental manipulation of the LC. Consequently, we hypothesized that there are several output pathways through which the LC is connected to the prepulse inhibition-mediating circuitry. One of them is the coerulean projection to the pedunculopontine tegmental nucleus that inhibits the primary startle circuit at the level of the pontine reticular nucleus (Jones 1991; Fendt et al. 2001; Alsene and Bakshi 2011). Another one is the coerulean projections to auditory nuclei that are involved in the prepulse inhibition such as the inferior colliculus (Hormigo et al. 2012; Yeomans et al. 2006) and the ventral nucleus of the trapezoid body which modulates CRN neuronal activity (Mulders and Robertson 2001; Gómez-Nieto et al. 2008a, 2013). In sum, the existence of direct projections from the LC to the cochlear root nucleus establishes the LC as an essential structure in the neuronal substrates underlying survival and escape behavioral paradigms in response to unexpected loud sounds.

Evidence of sexual dimorphism in the LC–noradrenergic system of the cochlear root nucleus

An interesting feature of the acoustic startle reflex and its prepulse inhibition is that human and rats show a marked sexual dimorphism, in which both behavioral paradigms are greater in males than in females (Lehmann et al. 1999; Braff et al. 2001; Aasen et al. 2005). However, little is known about the neuronal mechanisms underlying these gender differences. Our study proposed the LC as an important structure in the modulation of the acoustic startle reflex that could be involved in the prepulse inhibition paradigm via the LC-CRN noradrenergic projection. Therefore, it was interesting to find out whether the adrenoreceptors in the cochlear root nucleus are expressed in a gender-based fashion. Our RT-qPCR data showed robust gender differences in the expression levels of adrenoreceptors such as $\alpha 1$, $\alpha 2$, $\beta 2$ subunits, and suggest that the

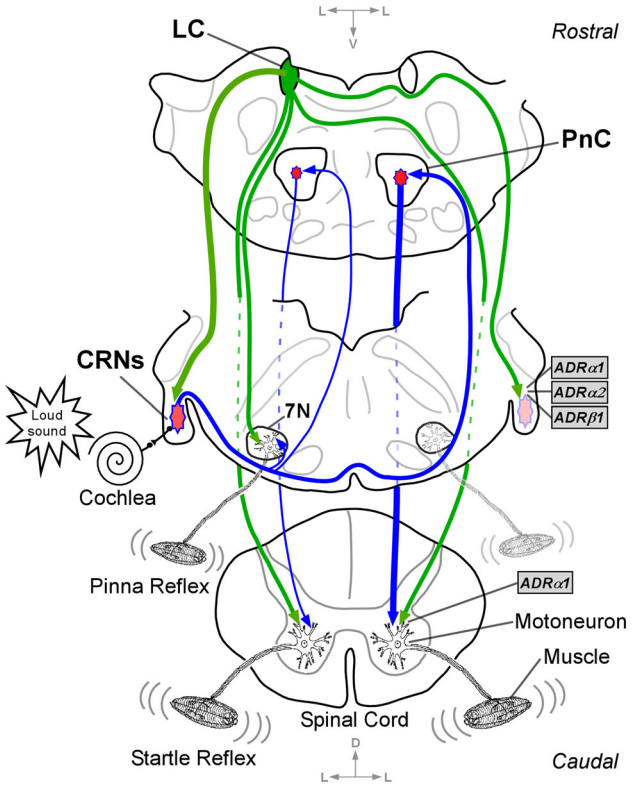

Fig. 11 Schematic drawing of the projections from locus coeruleus (LC) to the primary acoustic startle and pinna reflex pathways. The primary acoustic startle circuit is represented in *blue* and the LC neuronal projections in *green*. First, a loud sound activates the auditory receptors in the cochlea. Next, auditory nerve fibers synapse cochlear root neurons (CRNs). Finally, CRNs convey short-latency acoustic input to neurons in the pontine reticular formation (PnC), whose axons finally contact motoneurons in the spinal cord to lead an acoustic startle reflex. The LC noradrenergic axons contact the primary acoustic startle reflex at the initial and final relays of the pathway. On the first relay, CRNs contain noradrenergic receptors ($\alpha 1$, $\alpha 2$, $\beta 2$-adrenoreceptors) that are sufficient to modulate the acoustic startle response. On the final relay, motoneurons in the spinal cord are under influence of excitatory projections from the LC via $\alpha 1$-adrenoreceptors. The CRNs also projects to motoneurons of the ipsilateral facial motor nucleus (7N) which, in turn, innervates the auricular muscles leading to the pinna reflex. The pinna reflex pathway is likely under the influence of the LC via the coerulean projections to CRNs and the facial motor nucleus. The line width represents side predominance and *arrowheads* indicate the flow of neuronal information within the circuit

effects of adrenoreceptor stimulation via LC-CRNs projection might be different between female and male rats. Since these adrenoreceptor subunits are known to be involved in prepulse inhibition (Carasso et al. 1998; Bakshi and Geyer 1999; Alsene et al. 2010; Szabadi 2012; Larrauri and Levin 2012), our results also suggest that the noradrenergic system of the cochlear root nucleus might contribute to the male–female differences observed in the behavioral paradigms. Although more experiments are needed to corroborate this, it is possible that the neuronal

substrates participating in the prepulse inhibition are slightly different in female and male rats. The LC–noradrenergic system has been reported to be sexually dimorphic at structural and functional levels (Guillamon et al. 1988; Luque et al. 1992; Curtis et al. 2006; Bangasser et al. 2010). Our 3D reconstruction analysis of the LC showed that the neuronal density clearly differs throughout the rostro-caudal length of the nucleus, with greater neuronal density in the rostral areas of the female LC than that in males. This finding could be related to the male–female differences observed in the structure of LC neurons including dendritic pattern as well as somatic volume and area which depend on its location within the nucleus (Luque et al. 1992; Bangasser et al. 2010). Taken together, our results suggest that the LC of female and male rats contains a distinct distribution of noradrenergic neurons that are accompanied with differences in adrenoreceptor stimulation at specific levels of the primary acoustic startle circuit as the cochlear root nucleus.

Acknowledgments We thank the two anonymous reviewers for their constructive comments, which helped us to improve the manuscript. This research was supported by grants from the Spanish Ministry of Science and Innovation (MICINN, #BFU2010-17754) to Dr. Dolores E. López and the São Paulo State Research Foundation (FAPESP, #2008/02771-6) to Dr. José de Anchieta de Castro e Horta-Júnior.

Conflict of interest The authors declare no competing financial interests.

References

Aasen I, Kolli L, Kumari V (2005) Sex effects in prepulse inhibition and facilitation of the acoustic startle response: implications for pharmacological and treatment studies. J Psychopharmacol 19(1):39–45

Adams LM, Geyer MA (1981) Effects of 6-hydroxydopamine lesions of locus coeruleus on startle in rats. Psychopharmacology 73(4):394–398

Aitkin L (1996) The anatomy of the cochlear nuclei and superior olivary complex of arboreal Australian marsupials. Brain Behav Evol 48:103–114

Alsene KM, Bakshi VP (2011) Pharmacological stimulation of locus coeruleus reveals a new antipsychotic-responsive pathway for deficient sensorimotor gating. Neuropsychopharmacology 36(8):1656–1667

Alsene KM, Fallace K, Bakshi VP (2010) Ventral striatal noradrenergic mechanisms contribute to sensorimotor gating deficits induced by amphetamine. Neuropsychopharmacology 35(12):2346–2356

Amaral DG, Sinnamon HM (1977) The locus coeruleus: neurobiology of a central noradrenergic nucleus. Prog Neurobiol 9:147–196

Aston-Jones G, Cohen JD (2005) Adaptive gain and the role of the locus coeruleus-norepinephrine system in optimal performance. J Comp Neurol 493:99–110

Aston-Jones G, Rajkowski J, Cohen J (1999) Role of the locus coeruleus in attention and behavioural flexibility. Biol Psychiatry 46:1309–1320

Bakshi VP, Geyer MA (1997) Phencyclidine-induced deficits in prepulse inhibition of startle are blocked by prazosin, an alpha-1 noradrenergic antagonist. J Pharmacol Exp Ther 283(2):666–674

Bakshi VP, Geyer MA (1999) Alpha-1-adrenergic receptors mediate sensorimotor gating deficits produced by intracerebral dizocilpine administration in rats. Neuroscience 92(1):113–121

Bangasser DA, Curtis A, Reyes BA, Bethea TT, Parastatidis I, Ischiropoulos H, Van Bockstaele EJ, Valentino RJ (2010) Sex differences in corticotropin-releasing factor receptor signaling and trafficking: potential role in female vulnerability to stress-related psychopathology. Mol Psychiatry 15(9):877, 896–904

Berridge CW, Abercrombie ED (1999) Relationship between locus coeruleus discharge rates and rates of norepinephrine release within neocortex as assessed by in vivo microdialysis. Neuroscience 93:1263–1270

Berridge CW, Waterhouse BD (2003) The locus coeruleus noradrenergic system: modulation of behavioral state and state dependent cognitive processes. Brain Res Rev 42:33–84

Braff DL, Geyer MA (1990) Sensorimotor gating and schizophrenia. Human and animal model studies. Arch Gen Psychiatry 47(2):181–188

Braff DL, Geyer MA, Swerdlow NR (2001) Human studies of prepulse inhibition of startle: normal subjects, patient groups, and pharmacological studies. Psychopharmacology 156(2–3):234–258

Cai J, Li J, Mao Y, Bai X, Xu L, Wang H (2013) Immunohistochemical localization of α2-adrenergic receptors in the neonatal rat cochlea and the vestibular labyrinth. J Mol Neurosci (Published online)

Carasso BS, Bakshi VP, Geyer MA (1998) Disruption in prepulse inhibition after alpha-1 adrenoceptor stimulation in rats. Neuropharmacology 37:401–404

Curtis AL, Bethea T, Valentino RJ (2006) Sexually dimorphic responses of the brain norepinephrine system to stress and corticotropin-releasing factor. Neuropsychopharmacology 31:544–554

Davis M, Cedarbaum JM, Aghajanian GK, Gendelman DS (1977) Effects of clonidine on habituation and sensitization of acoustic startle in normal, decerebrate and locus coeruleus lesioned rats. Psychopharmacology (Berl) 51(3):243–253

Ebert U (1996) Noradrenalin enhances the activity of cochlear nucleus neurons in the rat. Eur J Neurosci 8:1306–1314

Fendt M, Li L, Yeomans JS (2001) Brain stem circuits mediating prepulse inhibition of the startle reflex. Psychopharmacology 156:216–224

Foote SL, Bloom FE, Aston-Jones G (1983) Nucleus locus coeruleus: new evidence of anatomical and physiological specificity. Physiol Rev 63:844–914

Foote SL, Berridge CW, Adams LM, Pineda JA (1991) Electrophysiological evidence for the involvement of the locus coeruleus in alerting, orienting, and attending. Prog Brain Res 88:521–532

Fritschy JM, Grzanna R (1990) Distribution of locus coeruleus axons within the rat brain stem demonstrated by *Phaseolus vulgaris* leucoagglutinin anterograde tracing in combination with dopamine-beta-hydroxylase immuno-fluorescence. J Comp Neurol 293:616–631

Gómez-Nieto R, Rubio ME, López DE (2008a) Cholinergic input from the ventral nucleus of the trapezoid body to cochlear root neurons in rats. J Comp Neurol 506:452–468

Gómez-Nieto R, Horta-Júnior JA, Castellano O, Herrero-Turrión MJ, Rubio ME, López DE (2008b) Neurochemistry of the afferents to the rat cochlear root nucleus: possible synaptic modulation of the acoustic startle. Neuroscience 154:51–64

Gómez-Nieto R, Horta-Júnior JA, Castellano O, Sinex DG, López DE (2010) Auditory prepulse inhibition of neuronal activity in the rat cochlear root nucleus. In: Palmer AR, Meddis R, López

Poveda EA (eds) The neurophysiological bases of auditory perception. Springer, New York, pp 79–90
Gómez-Nieto R, Sinex DG, C Horta-Júnior JD, Castellano O, Herrero-Turrión JM, López DE (2013) A fast cholinergic modulation of the primary acoustic startle circuit in rats. Brain Struct Funct. Published online
Groves PM, Thompson RF (1970) Habituation. A dual process theory. Psycholo Rev 77(5):419–450
Guillamon A, de Blas MR, Segovia S (1988) Effects of sex steroids on the development of the locus coeruleus in the rat. Brain Res 468:306–310
Gupta A, Décaillot FM, Gomes I, Tkalych O, Heimann AS, Ferro ES, Devi LA (2007) Conformation state-sensitive antibodies to G-protein-coupled receptors. J Biol Chem 282(8):5116–5124
Harrison JM, Warr WB, Irving R (1962) Second order neurons in the acoustic nerve. Science 138:893–895
Hoffman HS, Ison JR (1980) Reflex modification in the domain of startle: I. Some empirical findings and their implications for how the nervous system processes sensory input. Psychol Rev 87:175–189
Hormigo S, Horta Júnior Jde A, Gómez-Nieto R, López DE (2012) The selective neurotoxin DSP-4 impairs the noradrenergic projections from the locus coeruleus to the inferior colliculus in rats. Front Neural Circuits 6:41
Horta-Júnior Jde A, López DE, Alvarez-Morujo AJ, Bittencourt JC (2008) Direct and indirect connections between cochlear root neurons and facial motor neurons: pathways underlying the acoustic pinna reflex in the albino rat. J Comp Neurol 507:1763–1779
Jones BE (1991) Noradrenergic locus coeruleus neurons: their distant connections and their relationship to neighboring (including cholinergic and GABAergic) neurons of the central gray and reticular formation. Prog Brain Res 88:15–30
Jones BE, Yang TZ (1985) The efferent projections from the reticular formation and the locus coeruleus studied by anterograde and retrograde axonal transport in the rat. J Comp Neurol 242(1):56–92
Klepper A, Herbert H (1991) Distribution and origin of noradrenergic and serotonergic fibers in the cochlear nucleus and inferior colliculus of the rat. Brain Res 557:190–201
Kritzer MF (2003) Long-term gonadectomy affects the density of tyrosine hydroxylase- but not dopamine-beta-hydroxylase-, choline acetyltransferase- or serotonin-immunoreactive axons in the medial prefrontal cortices of adult male rats. Cereb Cortex 13:282–296
Kromer LF, Moore RY (1976) Cochlear nucleus innervation by central norepinephrine neurons in the rat. Brain Res 118:531–537
Kromer LF, Moore RY (1980) A study of the organization of the locus coeruleus projections to the lateral geniculate nuclei in the albino rat. Neuroscience 5:255–271
Landis C, Hunt WA (1939) The startle pattern. Ferrar and Rinehart, New York
Larrauri JA, Levin ED (2012) The α2-adrenergic antagonist idazoxan counteracts prepulse inhibition deficits caused by amphetamine or dizocilpine in rats. Psychopharmacology 219(1):99–108
Lee Y, López DE, Meloni EG, Davis M (1996) A primary acoustic startle pathway: obligatory role of cochlear root neurons and the nucleus reticularis pontis caudalis. J Neurosci 16:3775–3789
Lehmann J, Pryce CR, Feldon J (1999) Sex differences in the acoustic startle response and prepulse inhibition in Wistar rats. Behav Brain Res 104(1–2):113–117
Li L, Du Y, Li N, Wu X, Wu Y (2009) Top-down modulation of prepulse inhibition of the startle reflex in humans and rats. Neurosci Biobehav Rev 33(8):1157–1167
Livak KJ, Schmittgen TD (2001) Analysis of relative gene expression data using real-time quantitative PCR and the 2(-Delta Delta C(T)). Methods 25:402–408
López DE, Merchán MA, Bajo VM, Saldaña E (1993) The cochlear root neurons in the rat, mouse and gerbil. In: Merchán MA, Juiz JM, Godfrey DA, Mugnaini E (eds) The mammalian cochlear nuclei: organization and function. Plenum Press, New York, pp 291–301
López DE, Saldaña E, Nodal FR, Merchán MA, Warr WB (1999) Projections of cochlear root neurons, sentinels of the auditory pathway in the rat. J Comp Neurol 415:160–174
Loughlin SE, Foote SL, Bloom FE (1986a) Efferent projections of nucleus locus coeruleus: topographic organization of cells of origin demonstrated by three-dimensional reconstruction. Neuroscience 18:291–306
Loughlin SE, Foote SL, Grzanna R (1986b) Efferent projections of nucleus locus coeruleus: morphologic subpopulations have different efferent targets. Neuroscience 18:307–319
Luque JM, de Blas MR, Segovia S, Guillamon A (1992) Sexual dimorphism of the dopamine-beta-hydroxylase-immunoreactive neurons in the rat locus ceruleus. Brain Res Dev Brain Res 67:211–215
Merchán MA, Collía F, López DE, Saldana E (1988) Morphology of cochlear root neurons in the rat. J Neurocytol 17:711–725
Molina V, Montes C, Tamayo P, Villa R, Isabel Osuna M, Pérez J, Sancho C, López-Albuquerque T, Cardoso A, Castellano O, López DE (2009) Correlation between prepulse inhibition and cortical perfusion during an attentional test in schizophrenia. A pilot study. Prog Neuropsychopharmacol Biol Psychiatry 33(1):53–61
Mulders WH, Robertson D (2001) Origin of the noradrenergic innervation of the superior olivary complex in the rat. J Chem Neuroanat 21:313–322
Nitecka L, Amerski L, Panek-Mikuła J, Narkiewicz O (1980) Tegmental afferents of the amygdaloid body in the rat. Acta Neurobiol Exp (Wars) 40(3):609–624
Nodal FR, López DE (2003) Direct input from cochlear root neurons to pontine reticulospinal neurons in albino rat. J Comp Neurol 460:80–93
Osen KK, López DE, Slyngstad TA, Ottersen OP, Storm-Mathisen J (1991) GABA-like and glycine-like immunoreactivities of the cochlear root nucleus in rat. J Neurocytol 20:17–25
Saitoh K, Shaw S, Tilson HA (1986) Noradrenergic influence on the prepulse inhibition of acoustic startle. Toxicol Lett 34:209–216
Samuels ER, Szabadi E (2008) Functional neuroanatomy of the noradrenergic locus coeruleus: its roles in the regulation of arousal and autonomic function part I: principles of functional organisation. Curr Neuropharmacol 6:235–253
Schmittgen TD, Livak KJ (2008) Analyzing real-time PCR data by the comparative C(T) method. Nat Protoc 3:1101–1108
Simpson KL, Altman DW, Wang L, Kirifides ML, Lin RC, Waterhouse BD (1997) Lateralization and functional organization of the locus coeruleus projection to the trigeminal somatosensory pathway in rat. J Comp Neurol 385(1):135–147
Sinex DG, López DE, Warr WB (2001) Electrophysiological responses of cochlear root neurons. Hear Res 158:28–38
Swerdlow NR, Geyer MA (1998) Using an animal model of deficient sensorimotor gating to study the pathophysiology and new treatments of schizophrenia. Schizophr Bull 24:285–301
Swerdlow NR, Geyer MA, Braff DL (2001) Neural circuit regulation of prepulse inhibition of startle in the rat: current knowledge and future challenges. Psychopharmacol 156:194–215
Szabadi E (2012) Modulation of physiological reflexes by pain: role of the locus coeruleus. Front Integr Neurosci 6:94
Szabadi E (2013) Functional neuroanatomy of the central noradrenergic system. J Psychopharmacol 27(8):659–693

Unnerstall JR, Kopajtic TA, Kuhar MJ (1984) Distribution of alpha 2 agonist binding sites in the rat and human central nervous system: analysis of some functional, anatomic correlates of the pharmacologic effects of clonidine and related adrenergic agents. Brain Res 319(1):69–101

Vicentic A, Robeva A, Rogge G, Uberti M, Minneman KP (2002) Biochemistry and pharmacology of epitope-tagged alpha(1)-adrenergic receptor subtypes. J Pharmacol Exp Ther 302(1):58–65

Yeomans JS, Lee J, Yeomans MH, Steidl S, Li L (2006) Midbrain pathways for prepulse inhibition and startle activation in rat. Neuroscience 142:921–929